

Research article

A method of gas-related pollution source layout based on multi-source data:
A case study of shaanxi province, China



Ying Yang ^{a,1}, Xin Xu ^{a,1}, Jing Wei ^c, Qian You ^d, Jun Wang ^e, Xin Bo ^{a,b,*}

^a Department of Environmental Science and Engineering, Beijing University of Chemical Technology, Beijing, 100029, PR China

^b BUCT Institute for Carbon-Neutrality of Chinese Industries, Beijing, 100029, PR China

^c Department of Atmospheric and Oceanic Science, Earth System Science Interdisciplinary Center, University of Maryland, College Park, USA

^d School of Management and Engineering, Capital University of Economics and Business, Beijing, 100070, PR China

^e Beijing Presky Technology Co., Ltd, Beijing, 100195, PR China

ARTICLE INFO

Handling Editor: Jason Michael Evans

Keywords:

Pollutant emission inventory
Atmospheric self-purification capacity
Satellite remote sensing air quality data
Moran's I index
Enterprise layout site selection

ABSTRACT

The location and layout of enterprises have an important impact on local air quality. However, a few studies on exploring of the optimal layout of gas-related enterprises from the perspective of optimizing the layout of air pollution sources. This study developed a method for the evaluation of air pollution source layout based on air pollutant emission inventory data, atmospheric self-purification capacity data, and satellite remote sensing air quality data. Taking Shaanxi Province as an example, the Moran's I index and GIS spatial analysis techniques were used to evaluate the layout of air pollution sources, analyze the spatial variation characteristics of air pollution sources, and propose specific countermeasures to optimize the layout of air pollution sources. Results showed that northern Shaanxi and Guanzhong Plain are the most unsuitable for the distribution of NO_x and CO sources, accounting for 13.78% and 21.77% of the total area, respectively. The most suitable area for the distribution of NO_x is southern Shaanxi, accounting for 65.77% of the total area, mainly concentrated in Hanzhong and Ankang regions. The most suitable area for the distribution of CO is southern Shaanxi, accounting for 40.97% of the total area, mainly concentrated in Hanzhong and Shangluo regions. The findings of this study could supplement and improve the evaluation of the layout of industrial enterprises in China from technical and methodological aspects, and provide new insight for local governments to adjust and optimize the layout of air pollution sources.

1. Introduction

In recent years, air pollution in China became a major economic and social issue across the country due to rapid economic growth, accelerated industrialization, and rapid urbanization (Li et al., 2022; Wang et al., 2022a). The reason was attributed to the influence of local industrial structure, layout, and energy consumption, especially in the rapidly growing industrial cities (Yang and Teng, 2018; Xue et al., 2023). For example, Linyi, as the logistics plate capital of China, had a significant impact on the local non-methane hydro-carbon (NMHC) concentration and formation of O₃ due to the significant differences in industrial structure and geographical location (Wang et al., 2022b). Yang (2022) explored the impact of industrialization on environmental pollution in different provinces of China, and the results showed that

industrial layout had an impact on environmental pollution (Yang, 2022). Obviously, the long-term industrial development not only promoted economic growth but also produced a large number of industrial pollutants, causing serious damage to the ecological environment (Ji et al., 2021; Li et al., 2022). Therefore, it is very important to take appropriate methods to accurately identify pollution sources, and then rationally plan the layout of heavy polluting enterprises for reducing air pollution and improving the image of the city.

At present, most research focused on pollutant control technologies and emission reduction strategies to achieve air quality improvement and environmental restoration. The essence of those approaches was to control air quality by reducing pollutant emissions. Another approach was to optimize the layout of air pollution sources, thereby taking advantage of the dilution and purification characteristics of the

* Corresponding author. BUCT Institute for Carbon-Neutrality of Chinese Industries, Beijing, 100029, PR China.

E-mail address: boxin@buct.edu.cn (X. Bo).

¹ These authors contributed equally to this paper.

atmosphere to reduce the harm of air pollution, and avoid the economic losses associated with reducing emissions to some extent, which was substantial to heavily polluted cities for the adjustment of the industrial layout. Various methods were adopted to consider pollutant emissions in existing systems for the evaluation of pollution source layout. From the meteorological perspective, previous studies mainly selected improved layout schemes based on traditional analysis of prevailing winds or the results of simple models (Zhu et al., 2022; Mo et al., 2023). Other studies combined air pollutant emission inventories and air quality models to research the impact of pollutants on the atmospheric environment under different planning scenarios, thereby providing a strategy for the optimization of enterprise layout (Tang et al., 2019). Additionally, the technique of satellite retrieval had unique advantages in assisting pollutant accounting, which has been proven helpful in guiding the optimized layout of enterprises (Alvarez-Mendoza et al., 2018; Biuki et al., 2022). However, those earlier studies relied on a single dataset and had certain limitations for compromising the scientific optimization of enterprise layout. Furthermore, most current studies used meteorological or emission inventories combined with air quality models to explore the optimal layout for a particular business or industry. However, for a city, it is necessary to systematically explore the optimal layout of enterprises in the whole city from the perspective of the whole city. Therefore, from the perspective of cities, multi-source data such as atmospheric self-purification capacity data, satellite remote sensing air quality data, and pollutant emission inventory data should be comprehensively considered to objectively reflect the current situation of air pollution under the existing layout of air pollution sources, and provide references for the layout and location of enterprises.

Shaanxi was an economically important province in Northwest China. Its gross domestic product (GDP) reached 218.981 billion yuan in 2017, and the output value of its secondary industry accounted for 49.8% of the total output value (National Bureau of Statistics of China Published NBSC, 2018). Shaanxi has made notable contributions to the formation of a complete national economic system and socioeconomic

development in China owing to its relatively complete heavy industry sector. However, the excessive development of heavy industry has brought substantial environmental pollution. Therefore, the research was devoted to resolving Shaanxi's air pollution issues and providing possible solutions which could contribute to easing the pressure of environmental management. This study was based on multi-source data (BUCT, 2023) for air pollution source layout optimization. Furthermore, this study analyzed the current situation of the layout of regional air pollution sources, evaluated the spatial variation characteristics of air pollution sources, and proposed targeted adjustment countermeasures for air pollution source layout. This study's findings would contribute to improving the method for evaluating China's industrial layout, and provide reference for relevant authorities regarding enterprise management.

2. Materials and methods

2.1. Study area

Shaanxi is in the hinterland of China ($31^{\circ}42' \text{--} 39^{\circ}35' \text{N}$, $105^{\circ}29' \text{--} 111^{\circ}15' \text{E}$) and represents an important node in the "Belt and Road" strategy. The study area includes 10 prefecture-level cities (Fig. 1), covering a total land area of about $20.56 \times 10^4 \text{ km}^2$ (Shaanxi Provincial Bureau of Statistics Published, 2018). In 2018, according to a study on air quality in 169 major cities in China, the cities of Xi'an and Xianyang in Shaanxi ranked in the bottom 20 in terms of air quality (MEEP, 2018). Due to factors such as terrain and atmospheric self-purification ability, there are five cities and two districts in Shaanxi province in the air pollution transmission corridor of Fen-Wei Plain region. The topography of Shaanxi was complex and can be divided into three categories from the south to the north, including southern Shaanxi Qinling Bashan Mountains (Hanzhong, Ankang, and Shangluo), central Shaanxi Guanzhong Plain (Baoji, Xi'an, Xianyang, Tongchuan, Weinan, and other cities) and northern Shaanxi Loess Plateau (Yulin and Yan

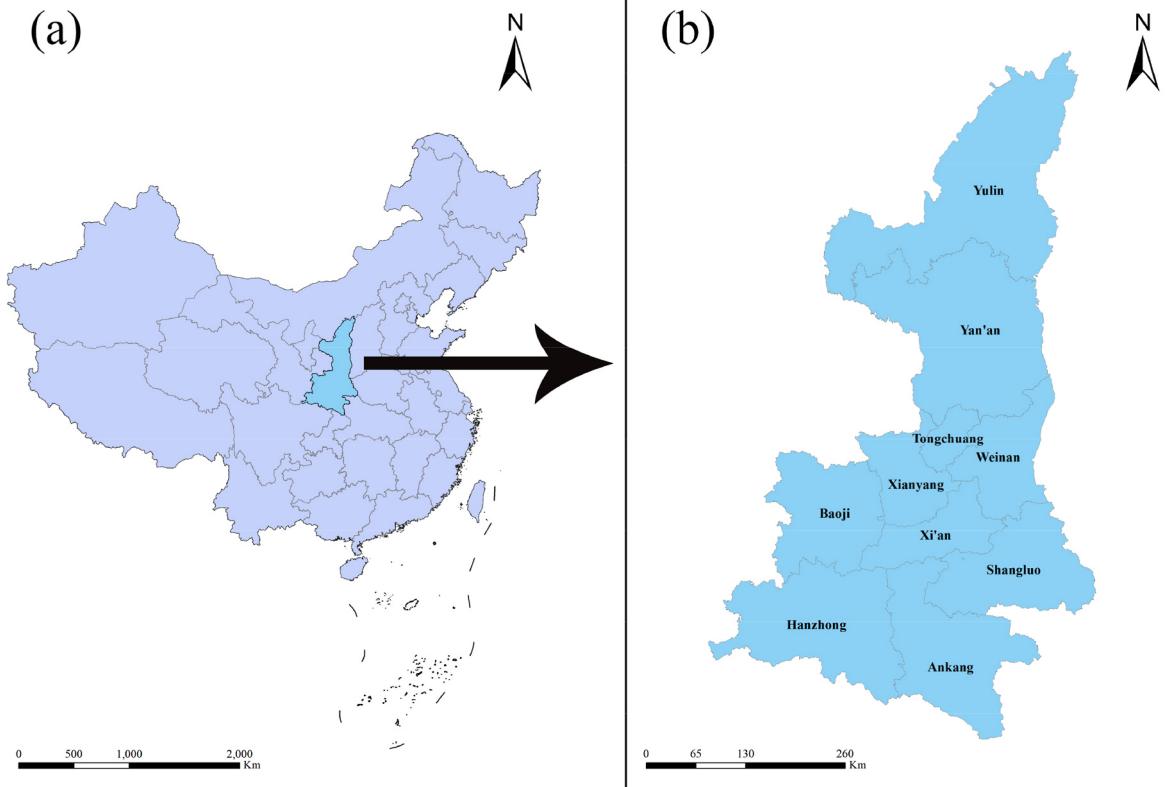


Fig. 1. Geographical location of the study area.

'an). Besides, Shaanxi spanned three different climatic zones, and the marked variation in climate from the north to the south results in the distinct difference in the self-purification capacity of the atmosphere in the different zones.

2.2. Data description

This study used three datasets (high-resolution pollutant emission inventory data, atmospheric self-purification capacity data, and satellite remote sensing air quality data) to establish the air pollution source optimization layout model for Shaanxi Province, and the structure, resolution, and format of the data were optimized and processed as described in subsections 2.2.1–2.2.3.

2.2.1. Atmospheric self-purification capacity data

Atmospheric self-purification capacity is a comprehensive representation of the inherent ability of the atmosphere to disperse, dilute, and deposit atmospheric pollutants, which has nothing to do with the emission of atmospheric pollution sources. Therefore, it can be used to quantify the contribution of changes in meteorological conditions to atmospheric pollution and to evaluate the effectiveness of air pollution control measures. Furthermore, it plays a key role in the prediction of the future potential of air pollution, providing a basis for early implementation of air pollution control measures (Chen et al., 2020b).

The atmospheric self-purification capacity data used in this study were obtained from the Local Analysis and Prediction System National Weather Service high-resolution (3-km grid) data compiled by the Public Weather Service. The data covered the region of 11°–54°N, 60°–140°E. Key data elements included hourly total cloudiness, low cloudiness, u-component wind speed at 10-m height, v-component wind speed at 10-m height, and 1-h accumulative precipitation (Bo et al., 2019). The calculation method used in this study referred to the National Standard of the People's Republic of China (GB/T 34,299–2017) (CMA, 2017), and the evaluation of the atmospheric self-purification capacity index (A) is accomplished using the following formula. The average atmospheric self-purification capacity index of Shaanxi Province in 2018 was calculated.

$$A = 3.1536 \times 10^{-3} \times \frac{\sqrt{H}}{2} \times V + 1.7 \times 10^{-2} \times R \times \sqrt{S} \quad (1)$$

where V is the ventilation volume (unit: m^2/s), R signifies precipitation intensity (unit: mm/d), and S means the unit area (unit: 100 km^2). The specific calculation steps are as follows:

- ① Firstly, the sun altitude Angle at each grid observation time is calculated;
- ② According to the total cloud cover/low cloud cover and solar altitude Angle, the solar radiation level is obtained by looking up the table;
- ③ According to the surface wind speed (calculated by the u component of the wind speed at 10 m high and the v component of the wind speed at 10 m high) and the solar radiation level, the Pasquill atmospheric stability level is obtained from the table;
- ④ Calculate the height of the mixed layer according to the level of atmospheric stability. Firstly, the region sequence number is determined according to the province where Shaanxi province is located, and then the thermal mixed layer coefficient a or mechanical mixed layer coefficient b of the region's serial number is obtained under different atmospheric stability levels by looking up the table, and the height of the mixed layer is calculated according to the following formula.

The height L_b of the thermal mixing layer is calculated under unstable and neutral meteorological conditions (the level of atmospheric stability for A, B, C, and D). The calculation formula is as follows:

$$L_b = a \times \frac{u_{10}}{f} \quad (2)$$

$$f = 2\Omega \sin\varphi \quad (3)$$

Where a is the coefficient of the thermal mixed layer; u_{10} is the average wind speed at a height of 10 m, expressed in meters per second (m/s). If it is greater than 6 m/s , the value is set to 6 m/s . f is the geostrophic parameter, expressed in degrees ($^\circ$); Ω is the angular speed of the Earth's rotation, expressed in degrees per second ($^\circ/\text{s}$). φ is geographical latitude in degrees ($^\circ$).

The mechanical mixing layer height is calculated under stable meteorological conditions (when the atmospheric stability is E and F), and the calculation formula is as follows:

$$L_b = b \times \sqrt{\frac{u_{10}}{f}} \quad (4)$$

Where b is the coefficient of mechanical mixing layer.

- ⑤ Calculate the wind speed at a height of 200 m according to the atmospheric stability and wind speed at a height of 10 m;

The average wind speed at the height of 10 m of the meteorological station is taken as the starting point, the wind speed below 200 m increases with the height according to the exponential law, and the wind speed above 200 m until the top of the mixing layer is taken as a constant, that is, the wind speed formula below 200 m is shown in the following formula:

$$u = u_{10} \times \left(\frac{z}{10}\right)^{P_m} \quad (5)$$

Where Z is the height in meters (m); u_{10} is the average wind speed at a height of 10 m, expressed in meters per second (m/s); When the value is greater than 6 m/s , it is 6 m/s . P_m is the Profile index of the vertical distribution of wind speed corresponding to different atmospheric stability, see Table 1, the classification of atmospheric stability, see Appendix B of the National Standard of the People's Republic of China (GB/T 34,299–2017).

- ⑥ Calculate the ventilation volume according to the height of the mixing layer, the wind speed at the height of 200 m and the wind speed at the height of 10 m;

When the height of the mechanical mixing layer is less than 200 m, the ventilation volume is calculated using the following formula:

$$V_E = (u_{200} + u_{10}) \times 0.5 \times L_b \quad (6)$$

Where V_E is the Ventilation volume, in square meters per second (m^2/s); u_{200} is the wind speed at an altitude of 200 m, in meters per second (m/s); u_{10} is the wind speed at altitude of 10 m, expressed in meters per second (m/s); L_b is the thermal or mixed layer height, in meters (m).

When the height of the thermal or mechanical mixing layer is more than 200 m, the ventilation volume is calculated using the following formula:

$$V_E = 200 \times (u_{200} + u_{10}) \times 0.5 + (L_b - 200) \times u_{200} \quad (7)$$

Where V_E is the ventilation volume, in square meters per second (m^2/s); u_{200} is the wind speed at an altitude of 200 m, in meters per second (m/s).

Table 1

Profile indices corresponding to different atmospheric stability.

Atmospheric stability classification	A	B	C	D	E	F
Profile index	0.07	0.07	0.1	0.15	0.25	0.25

s); u_{10} is the wind speed at altitude of 10 m, expressed in meters per second (m/s); L_b is the thermal or mixed layer height, in meters (m).

- ⑦ Calculate the atmospheric self-purification capacity index and grade of each time according to the calculation formula of atmospheric self-purification capacity index.

2.2.2. Satellite remote sensing air quality data

The satellite remote sensing air quality data with high quality and high resolution used in this study were collected from the ChinaHigh-AirPollutants (CHAP) dataset (Wei et al., 2022; Wei et al., 2023). This dataset was generated from big data that integrate ground-based observations, satellite remote sensing products, atmospheric reanalysis, and model emission inventories to infer surface concentrations of particulate and gaseous air pollutants using artificial intelligence technology. This study employed the surface NO₂ and CO data at a spatial resolution of 10 km × 10 km (Wei et al., 2022; Wei et al., 2023). In subsequent studies, it was divided into a grid with a resolution of 3 km × 3 km.

2.2.3. Pollutant emission inventory

A pollutant emission inventory represents the quantitative characterization of various pollutants discharged into the atmosphere by pollution sources within a certain temporal span and over a certain spatial range. A high-resolution air pollutant discharge inventory represents the basic data of air quality management, and such information was vital to the study of air pollution formation mechanisms, pollution control strategies, air quality early warning, and prediction.

The method adopted in this study for the compilation of the pollutant emission inventory referred to the high-resolution emission inventory of Hainan Province in 2017, as described in our previous research (Xu et al., 2023). The spatial resolution of the inventory is 3 km × 3 km and the emission sources are subdivided into fossil fuel combustion sources, process sources, solvent use sources, on-road mobile sources, non-road mobile sources, agricultural sources, dust, storage, and transportation sources, and waste treatment sources. The data source referred to the “three lines one permit” of Shaanxi Province compiled in previous research (Chen et al., 2020a). The dataset includes 7 pollutants: SO₂, NO_x, CO, PM₁₀, PM_{2.5}, VOCs, and NH₃. The compiled pollutant emission inventory of Shaanxi Province comprehensively and objectively reflects the current air pollution situation, and supports research on regional air pollution sources, pollution formation mechanisms, and air pollution prediction, thereby providing a reference for air pollution prevention and control strategies, and formulation of pollution control measures.

2.3. Distribution model of atmospheric pollution sources based on multi-source data

2.3.1. Spatial autocorrelation analysis of pollutants emission source

Spatial autocorrelation analysis was performed to understand the spatial dependence of the different types of datasets. Spatial correlation referred to the calculation of the degree of spatial autocorrelation between a spatial unit and its surrounding units for a certain eigenvalue, through the application of statistical methods to analyze the characteristics of the spatial distribution of the spatial units (Song et al., 2020; Shi et al., 2023). The Moran's I index has been widely used in spatial autocorrelation analysis (Zhang et al., 2008; Zhao et al., 2022). The value of Moran's I index was between -1 and +1. A value of the Moran's I index of >0 indicated that high (low) values were clustered together with other high (low) values, and thus the data present positive spatial autocorrelation. Conversely, a value of the Moran's I index of <0 indicated that high values are clustered together with low values, and thus the data presented negative spatial autocorrelation. A value of the Moran's I index close to 0 signified that high and low values were distributed randomly and exhibit no spatial autocorrelation. The Moran's I index can be divided into a global index and a local index. The

global Moran's I index was used to indicate whether attribute values are clustered in space, and the local Moran's I index further indicated the clustering area of high or low attribute values. The specific calculation methods for the global and local indexes are as follows:

$$I = \frac{n \times \sum_{i=1}^n \sum_{j=1}^n w_{i,j} (x_i - \bar{x})(x_j - \bar{x})}{\sum_{i=1}^n \sum_{j=1}^m w_{i,j} \times \sum_{i=1}^n (x_i - \bar{x})^2} \quad (8)$$

$$I_L = \frac{n \times (x_i - \bar{x}) \sum_{j=1}^n w_{i,j} (x_j - \bar{x})}{\sum_{i=1}^n \sum_{j=1}^m w_{i,j} \times \sum_{i=1}^n (x_i - \bar{x})^2} \quad (9)$$

where I is the global Moran's I index; I_L is the local Moran's I index; x_i and x_j signify the attribute values at locations i and j , respectively; \bar{x} is the average of the attribute values at all points i and j ; n denotes the number of all study objects; and w_{ij} represents the weight assigned to each raster measurement cell.

The significance test of the calculated Moran's I index was performed using the Z-distribution and it was determined as follows:

$$Z = \frac{I - E(I)}{\sqrt{Var(I)}} \quad (10)$$

where $Var(I)$ is the variance of the global Moran's I index, and $E(I)$ signifies the expected value of the global Moran's I index. When $|Z| > 2.58$, it means that the element has a significant aggregation or dispersion characteristic in the 99% confidence interval; otherwise, it is distributed randomly.

2.3.2. Assessment of the layout of atmospheric pollution sources

Based on natural factors such as meteorological diffusion conditions and the geographical features of Shaanxi, combined with pollutant emission intensity and satellite remote sensing air quality data, this study identified areas where the layout of pollution sources might have a serious impact on regional air quality and determined evaluation criteria of air pollution sources. Furthermore, three different datasets were processed and graded according to certain proportions; datasets with proportions of 0%–33%, 33%–67%, and 67%–100% were defined as a large class, medium class, and small class, respectively. Grids that met the requirements of large atmospheric self-cleaning capacity data, small pollutant emission inventory data, and small satellite remote sensing air quality data were classified as grids with better atmospheric capacity, which were considered most suitable for enterprise layout and could accommodate more atmospheric pollution sources (e.g., factories, industrial parks, and traffic sources). Conversely, grids that met the requirements of small atmospheric self-cleaning capacity data, large pollutant emission inventory data, and large satellite remote sensing air quality data were classified as grids with poor atmospheric capacity, which were considered unsuitable for the layout of enterprises and unable to accommodate more atmospheric pollution sources. The remaining grids were defined as those with general atmospheric environmental capacity (Table S1).

3. Results and discussion

3.1. Spatial distribution characteristics

3.1.1. Current status of pollutant emissions in cities

The spatial distributions of high-value regions of CO and NO_x were mainly concentrated in the Guanzhong Plain area, and Yulin City in northern Shaanxi, and overlapping features existed in most sites, indicating that NO_x and CO were spatially homogeneous (Fig. 2). The NO_x and CO emissions in Guanzhong accounted for 49.2% and 48.05% of the

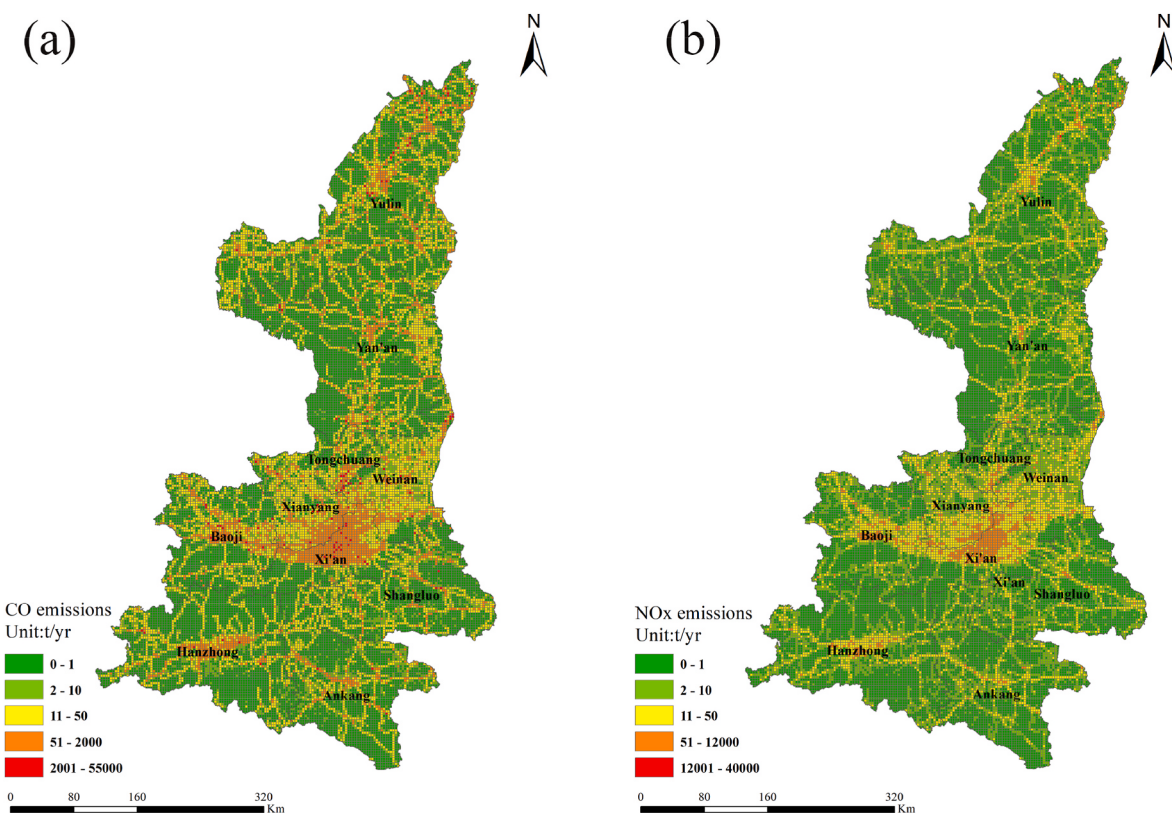


Fig. 2. Spatial emission distribution characteristics of (a) CO and (b) NO_x at 3 km × 3 km resolution in Shaanxi in 2017.

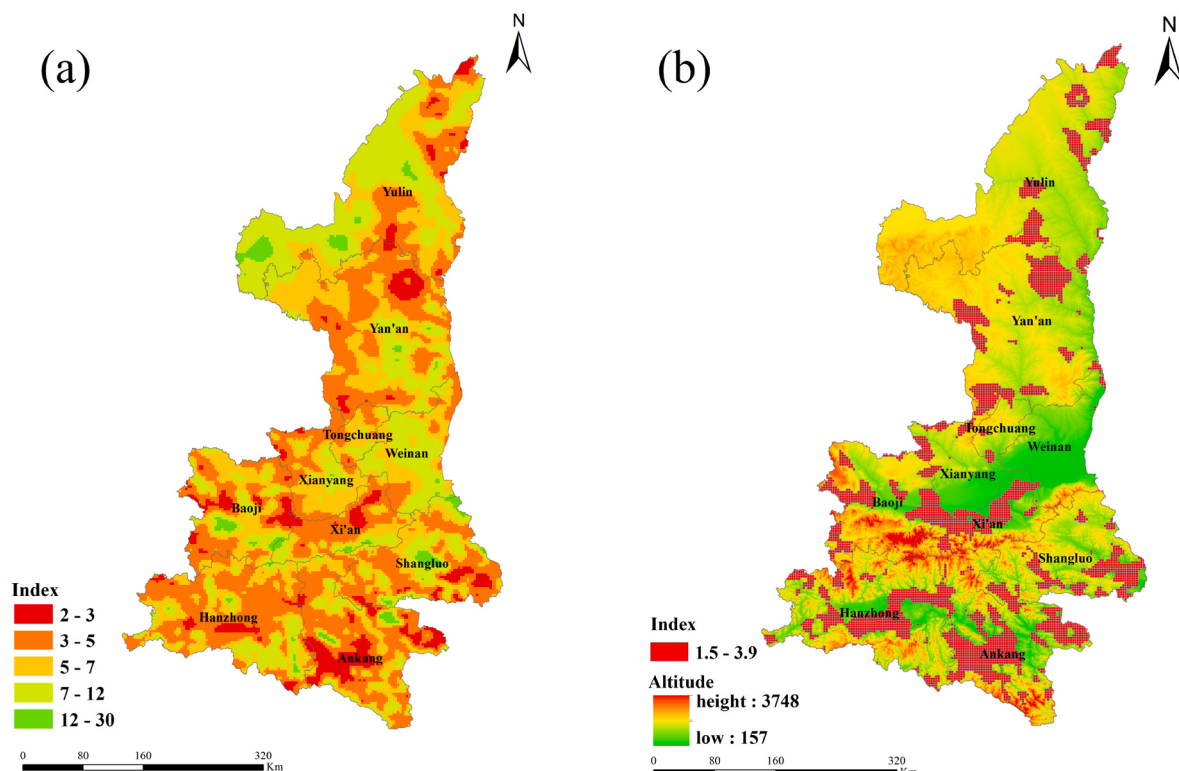


Fig. 3. (A) Distribution map of atmospheric self-purification capacity index in Shaanxi Province in 2018 (b) distribution of weak atmospheric dispersion zones superimposed on the terrain of Shaanxi Province.

total in Shaanxi, respectively, and Yulin's NO_x and CO emissions accounted for 32.09% and 29.24% of the total, respectively (Table S2). Fossil fuel combustion sources contributed a significant amount of NO_x emissions (45.05% of the total NO_x emissions), which was followed by mobile sources (35.60%). Fossil fuel combustion sources were also the largest contributor to CO emissions, accounting for 43.39% of total CO emissions, followed by industrial process sources (32.89%), and mobile sources (22.57%) (Table S3). Furthermore, NO_x emissions were mainly from power plants, accounting for 60.72% of the total emissions. The majority of CO emissions came from mining and manufacturing, which accounted for 53.65% of total emissions, followed by power plants (21.84%) (Table S4) (Wang, 2020).

3.1.2. Status of atmospheric self-purification capacity index

Based on the mean value of atmospheric environment diffusion index in Shaanxi Province in 2018, the grid or region with small atmospheric environment diffusion index value is selected as the weak atmospheric environment diffusion region according to certain threshold value or proportional value. Since there is no uniform threshold standard for weak diffusion, different proportions such as 10%, 15%, 20%, 25% in reverse order of atmospheric diffusion index can be used as the basis for the classification of weak diffusion in atmospheric environment (Zhu et al., 2018; Chen et al., 2020b). In this study, the atmospheric weak diffusion zone is defined by 20% of the atmospheric diffusion index ranking in reverse order of Shaanxi Province. The distribution of the atmospheric self-purification ability index and the atmospheric weak diffusion zone of Shaanxi Province in 2018 are shown in Fig. 3. Areas of weak diffusion of the atmospheric environment were mainly distributed over plains, basins, river valleys, leeward slopes of foothills, and other low-elevation areas, mainly in the range of 200–1000 m. The main reason was attributed to Shaanxi's complex topography, including the Beishan Mountains, Qinling Mountains, Daba Mountains, and other major mountain ranges. There was a large relative topographic difference between the plains and basins in the valley bottoms and the mountains that form a curtain that has an obvious blocking effect on

airflow, thereby promoting the formation of areas of low wind speed in Guanzhong Basin, Hanzhong Basin, and some areas of the northern Shaanxi Plateau (Xu et al., 2017). Moreover, the mountains restrict the ventilation diffusion and flow transport capacity of the atmosphere, thus forming weak diffusion zones of the atmospheric environment.

3.1.3. Current status of satellite remote sensing data

Satellite remote sensing data of CO and NO_x in Shaanxi are displayed in Fig. 4. Areas of poor air quality were distributed over the Guanzhong Plain area and in northern Shaanxi (especially Yulin City), consistent with the analysis results shown in Fig. 2. Possible explanations for this distribution could be ascribed to the following. Firstly, the Guanzhong area had high population density (Fig. S1), high traffic flow (Fig. S2), and intense industrial activities, with population, vehicles, and GDP accounting for 63%, 74%, and 65% of the total in Shaanxi Province, respectively (Table 2), even though its area accounts for only 27% of the total area of Shaanxi Province. Secondly, Guanzhong Plain was within the weak atmospheric dispersion zone in Shaanxi, with serious emissions of atmospheric pollutants and relatively poor air quality, as mentioned earlier. Thirdly, northern Shaanxi was the base of the large-scale energy and chemical industry in the region, and it had played a vital role in the west–east coal transportation, west–east electricity transportation, and west–east gas transportation projects. Owing to the long-term dominance of industrial sources and the high emission of pollutants in northern Shaanxi, the satellite remote sensing data indicated that the air quality is poor, especially in Yulin City.

3.2. Correlation analysis

3.2.1. Univariate correlation analysis

Multi-source data (satellite remote sensing air quality data, pollutant emission inventory data, and atmospheric self-purification capacity data) were classified and sorted, and GeoDa software (version 1.18.0) was used to calculate the univariate Moran's I index of NO_x and CO. The NO_x and CO of these three datasets showed significant correlation at the

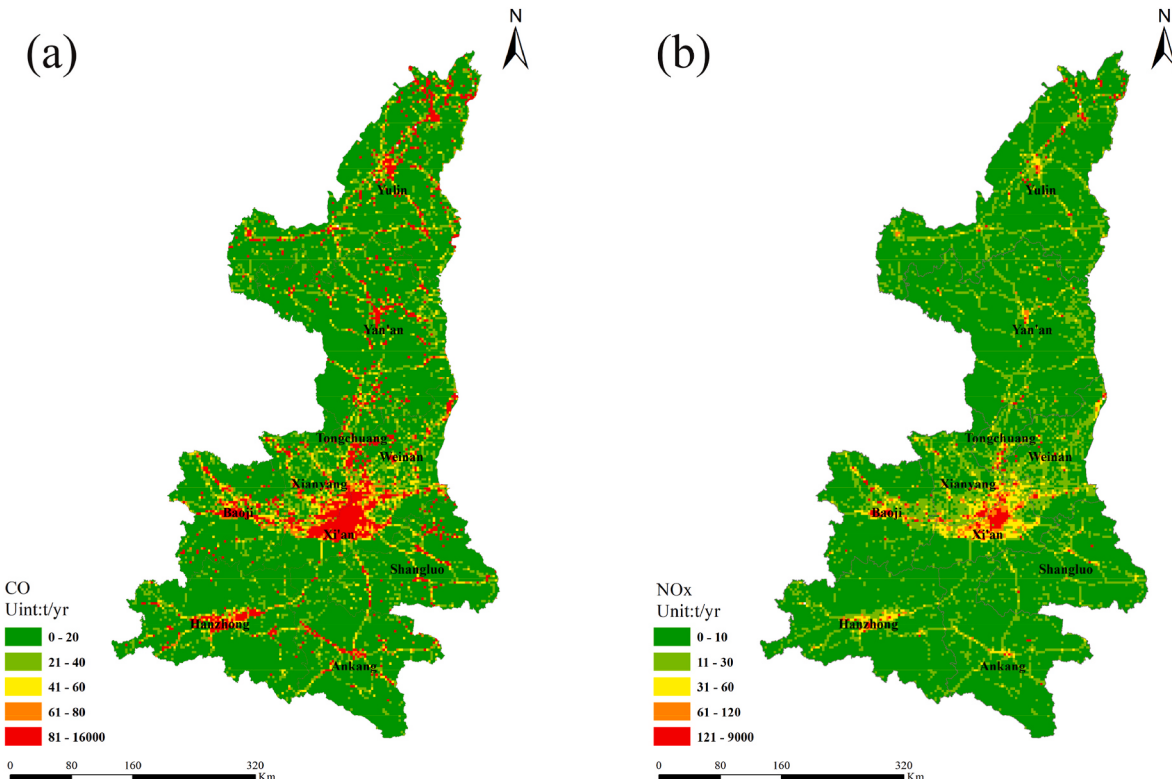


Fig. 4. Satellite remote sensing data map of 3km × 3 km of CO and NO_x in Shaanxi.

Table 2

Population, vehicle numbers, and GDP of the ten cities in Shaanxi during 2017.

City	Yulin	Yan'an	Baoji	Xi'an	Xianyang	Tongchuan	Weinan	Ankang	Hanzhong	Shangluo	Total
Area (Thousand square kilometer)	4.29	3.70	1.82	1.01	1.03	0.39	1.30	2.35	2.71	1.96	20.56
Population (million)	3.38	2.21	3.75	8.63	5.05	0.85	5.34	2.64	3.43	2.35	37.63
Vehicles (thousand)	510	246	205	1966	271	69	394	94	174	67	3996
GDP (billion yuan)	262.1	119.9	178.9	581	215.6	32.5	146.9	77.2	99.1	62.2	1775.4

Table 3

Univariate Moran's I index analysis of satellite remote sensing air quality data, pollutant emission inventory data, and atmospheric self-purification capacity data.

Dataset	Pollutant	I	P	Z
Satellite remote sensing air quality	NO _x	0.868	0.00001	260.98
	CO	0.815	0.00001	245.09
Pollutant emission inventory data	NO _x	0.032	0.001	13.48
	CO	0.047	0.00046	14.82
Atmospheric self-purification	/	0.933	0.00001	280.58

level of $P < 0.001$; the Z scores were all >2.58 , and the Moran's I index values were positive (Table 3). Thus, the distributions of NO_x and CO in the study area had clustering characteristics. The significance test of the univariate Moran's I index analysis signified statistical significance, which provided a theoretical basis for subsequent bivariate Moran's I index analysis.

3.2.2. Bivariate correlation analysis

In order to reflect the correlation between the satellite remote sensing dataset and the atmospheric self-purification capacity dataset more accurately, an adjacency spatial weight matrix was constructed using GeoDa software (version 1.18.0), and bivariate local Moran's I index analysis was conducted. The clustering types included the high values of atmospheric self-purification capacity data and the high values

of satellite remote sensing air quality data (H-H), the low values of atmospheric self-purification capacity data and the low values of satellite remote sensing air quality data (L-L), the high values of atmospheric self-purification capacity data and the low values of satellite remote sensing air quality data (H-L), and the low values of atmospheric self-purification capacity data and the high values of satellite remote sensing air quality data (L-H). Types H-H and L-L both denoted a region with the same data attributes as its surroundings, whereas types H-L and L-H both denoted a region surrounded by a region with different data attributes, and they were used to detect spatial heterogeneity.

The high level of satellite remote sensing air quality data was found to correlate with the low level of air self-purification capacity data, and vice versa. For NO_x and CO, H-L type areas were mainly distributed in Shaanxi's central and eastern urban clusters, and L-H type areas were mainly distributed in Shaanxi's northern and eastern urban clusters (Fig. 5), corresponding to the analysis results above.

3.3. Results of classification

GIS mapping can assess the layout of relevant air pollution sources by visualizing spatial patterns (Hao and Shen, 2022). According to the division criteria, Shaanxi was divided into three categories: green, indicating areas suitable for enterprise layout (high atmospheric environmental capacity), red, indicating areas unsuitable for enterprise layout (poor atmospheric environmental capacity), and blue, indicating

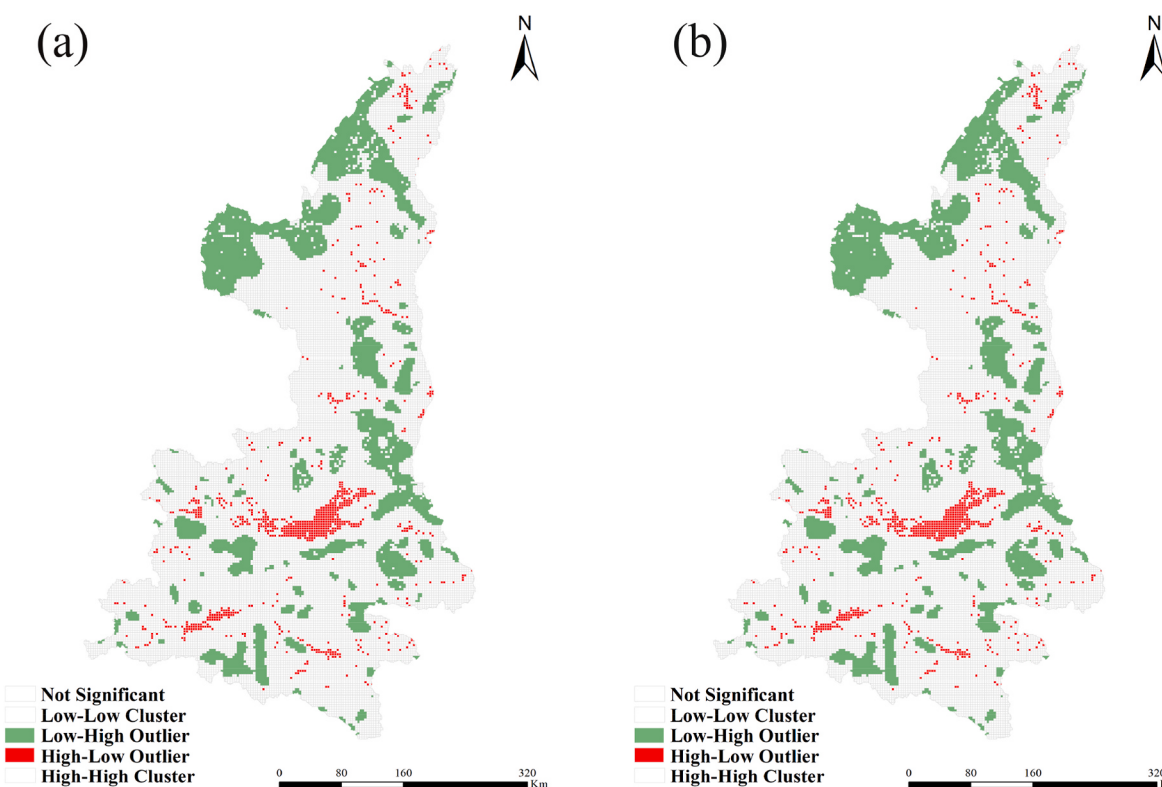


Fig. 5. Local indicators of spatial association cluster map of satellite remote sensing air quality data and atmospheric self-purification capacity data of (a) CO and (b) NO_x in Shaanxi.

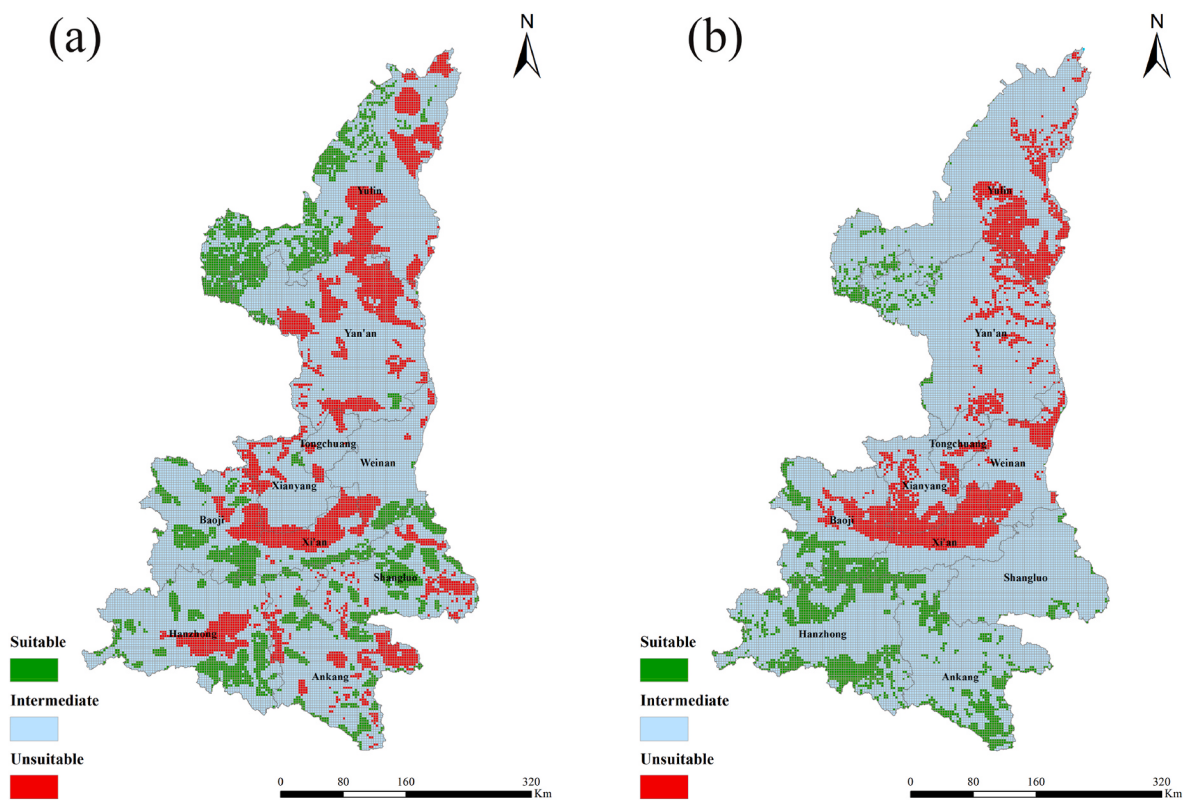


Fig. 6. The suitable, intermediate, and unsuitable enterprise layout map in Shaanxi Province considering CO (a) and NO_x (b), respectively (resolution:3 km × 3 km).

areas with intermediate suitability for enterprise layout (moderate atmospheric environmental capacity) (Fig. 6).

The results showed that the area proportion suitable for NO_x pollution sources was the smallest in northern Shaanxi Province (about 13.78%), and the largest in southern Shaanxi Province (about 65.77%), mainly concentrated in Hanzhong and Ankang regions. The area proportion unsuitable for NO_x pollution sources is Guanzhong Plain (about 56.49%), followed by northern Shaanxi Province (about 43.5%). The proportion of suitable area for CO pollution sources was the smallest in Guanzhong Plain (about 21.77%), the largest in southern Shaanxi (about 40.97%), mainly concentrated in Hanzhong and Shangluo, and the proportion of unsuitable area for CO pollution sources was the largest in northern Shaanxi (about 45.26%) (Table S5). This was consistent with the high level of urbanization on the Guanzhong Plain and the intense industrialization in Yulin city (northern Shaanxi). This study defined the spatial differentiation of environmental function attributes of each region in Shaanxi Province, which could provide new perspective and reference for relevant departments to reasonably determine the environmental quality objectives of subregions.

4. Conclusions

Using Shaanxi as a case example, this study innovatively developed a method for the layout of air pollution sources based on multi-source data. The results showed that the spatial distribution of high concentrations of CO and NO_x were mainly concentrated in Guanzhong Plain and Yulin City in northern Shaanxi Province. The NO_x and CO emissions in Guanzhong area accounted for 49.2% and 48.05% of the total amount of Shaanxi Province, respectively, and the NO_x and CO emissions in Yulin City accounted for 32.09% and 29.24% of the total amount of Shaanxi Province. Fossil fuel combustion source was the largest contributor to NO_x and CO emissions. The correlation analysis of the Moran's I index suggested that the emission source intensity of both NO_x and CO in Shaanxi was consistent with the trend of variation in pollutant

concentration determined from satellite remote sensing data. Overall, the largest proportions of areas suitable for the layout of NO_x and CO pollution sources were in southern Shaanxi, accounting for 65.77% and 40.97% of the total, respectively, indicating that southern Shaanxi areas were most suitable for the layout and site selection of enterprises.

The evaluation method based on the air pollutant emission inventory data, atmospheric self-purification capacity data, and satellite remote sensing air quality data was established, and it can more objectively reflect the current situation of air pollution under the air pollution source layout. The application of the proposed evaluation method could reduce not only the unreasonable distribution of existing industry and its negative impact on the environment but also the unreasonable restrictions of existing evaluation systems on local economic development, thereby improving local economic benefits.

CRediT authorship contribution statement

Ying Yang: Conceptualization, Methodology, Software, Writing – review & editing. **Xin Xu:** Conceptualization, Methodology, Software, Writing – review & editing. **Jing Wei:** Data curation, Supervision. **Qian You:** Data curation. **Jun Wang:** Conceptualization, Supervision. **Xin Bo:** Conceptualization, Funding acquisition, Supervision, Writing – review & editing, Resources.

Declaration of competing interest

The authors declare that they have no known competing financial interests or personal relationships that could have appeared to influence the work reported in this paper.

Data availability

Data will be made available on request.

Acknowledgments

This work was supported by grants from the National Natural Science Foundation of China (No. 72174125) and Fundamental Research Funds for the Central Universities (buctrc202133). The ChinaHighAirPollutants (CHAP) dataset is available at <https://weijing-rs.github.io/publication.html>.

Appendix A. Supplementary data

Supplementary data to this article can be found online at <https://doi.org/10.1016/j.jenvman.2023.119198>.

References

- Alvarez-Mendoza, C.I., Teodoro, A., Torres, N., et al., 2018. Comparison of satellite remote sensing data in the retrieve of PM10 air pollutant over Quito, Ecuador. *Remote Sens. Technol. Appl. In Urban Environ.* III, 10793 <https://doi.org/10.1117/12.2325324>.
- Biuki, Z.A., Parvin, P., Aghaei, M., 2022. Satellite remote sensing of particulate matter in the atmosphere of megacities: a case study of Tehran, Iran. *Atmos. Pollut. Res.* 13 (10), 101545 <https://doi.org/10.1016/j.apr.2022.101545>.
- Bo, X., Xue, X., Xu, J., et al., 2019. Aviation's emissions and contribution to the air quality in China. *Atmos. Environ.* 201, 121–131. <https://doi.org/10.1016/j.atmosenv.2019.01.005>.
- BUCT, 2023. A Method of Air Pollution Source Distribution Based on Multi-Source Data. Beijing University of Chemical Technology, CN202211679406.8 (in Chinese).
- Chen, L., Bo, X., Wang, T., Wang, Y., 2020a. Study on the atmospheric environment control unit division in Shaanxi "three lines one permit". *Environ. Impact Assess.* 42 (5), 11–15. <https://doi.org/10.14068/j.ceia.2020.05.003> (in Chinese).
- Chen, M., Li, Z.L., Lv, P.J., et al., 2020b. Methodology and practice for determining the weak diffusion zoning in chongqing. *Environ. Impact Assess.* 42 (6) <https://doi.org/10.14068/j.ceia.2020.06.016> (in Chinese).
- CMA, 2017. Grads of atmospheric self-purification capability. China Meteorol. Admin. https://www.cma.gov.cn/zfxgk/gknr/flgbz/bz/202209/t20220921_5099003.html. (Accessed 26 July 2023) (in Chinese).
- Hao, J.F., Shen, X.Y., 2022. Application of digital image processing and GIS technology in the evaluation of rationality of urban and rural planning spatial layout. *Secur. Commun. Network.* 2022, 1693706 <https://doi.org/10.1155/2022/1693706>.
- Ji, D.J., Zhou, P., Wu, F., 2021. Do marginal abatement costs matter for improving air quality? Evidence from China's major cities. *J. Environ. Manag.* 286, 1037–1046. <https://doi.org/10.1016/j.jenvman.2018.07.010>.
- Li, J., Hao, X., Liao, H., et al., 2022. Winter particulate pollution severity in North China driven by atmospheric teleconnections. *Nat. Geosci.* 15 (5), 349–355. <https://doi.org/10.1038/s41561-022-00933-2>.
- Ministry of Ecology and Environmental of the People's Republic of China Published MEEP, 2018. China Environmental Status Bulletin. https://www.mee.gov.cn/ywdt/pxw/201905/t20190529_704841.shtml. (Accessed 26 July 2023) (in Chinese).
- Mo, H., You, Y., Wu, L., et al., 2023. Potential impact of industrial transfer on PM(2.5) and economic development under scenarios oriented by different objectives in Guangdong, China. *Environ. Pollut.* 316, 120562 <https://doi.org/10.1016/J.ENVPOL.2022.120562>.
- National Bureau of Statistics of China Published NBSC, 2018. China Statistical Yearbook 2018. China Statistics Press Beijing.
- Shaanxi Provincial Bureau of Statistics Published, S.P.B.S., 2018. Shaanxi Statistical Yearbook 2018 Beijing. <http://tjj.shaanxi.gov.cn/tjj/ndsj/tjnjj/xttjnj/index.html?2018>. (Accessed 26 July 2023).
- Shi, H., Wang, P., Zheng, J., et al., 2023. A comprehensive framework for identifying contributing factors of soil trace metal pollution using Geodetector and spatial bivariate analysis. *Sci. Total Environ.* 857, 159636 <https://doi.org/10.1016/j.scitotenv.2022.159636>.
- Song, W., Wang, C., Chen, W., et al., 2020. Unlocking the spatial heterogeneous relationship between Per Capita GDP and nearby air quality using bivariate local indicator of spatial association. *Resour. Conserv. Recycl.* 160, 104880 <https://doi.org/10.1016/j.resconrec.2020.104880>.
- Tang, L., Qu, J., Mi, Z., et al., 2019. Substantial emission reductions from Chinese power plants after the introduction of ultra-low emissions standards. *Nat. Energy* 4 (11), 929–938. <https://doi.org/10.1038/s41560-019-0468-1>.
- Wang, T., 2020. Study on the Present Situation of Air Pollutants Emissions and Reduction Potential in Shaanxi. Xi'an University of Architecture and Technology, Xi'an (in Chinese).
- Wang, Y., Bai, Y., Zhi, X., et al., 2022a. Two typical patterns of regional PM2.5 transport for heavy air pollution over Central China: rapid transit transport and stationary accumulation transport. *Front. Environ. Sci.* 10, 890514 <https://doi.org/10.3389/fenvs.2022.890514>.
- Wang, G., Zhu, Z., Liu, Z., et al., 2022b. Ozone pollution in the plate and logistics capital of China: insight into the formation, source apportionment, and regional transport. *Environ. Pollut.* 313, 120144 <https://doi.org/10.1016/j.envpol.2022.120144>.
- Wei, J., Liu, S., Li, Z., et al., 2022. Ground-level NO₂ surveillance from space across China for high resolution using interpretable spatiotemporally weighted artificial intelligence. *Environ. Sci. Technol.* 56, 9988–9998. <https://doi.org/10.1021/acs.est.2c03834>.
- Wei, J., Li, Z., Wang, J., et al., 2023. Ground-level gaseous pollutants (NO₂, SO₂, and CO) in China: daily seamless mapping and spatiotemporal variations. *Atmos. Chem. Phys.* 23, 1511–1532. <https://doi.org/10.5194/acp-23-1511-2023>.
- Xu, H., Ying, Q., Hu, J., et al., 2017. Spatial and temporal variations in criteria air pollutants in three typical terrain regions in Shaanxi, China, during 2015. *Air Qual., Atmos. Health* 11, 95–109. <https://doi.org/10.1007/s11869-017-0523-7>.
- Xu, Z., Chen, S., Sang, M., et al., 2023. Air quality improvement through vehicle electrification in Hainan province, China. *Chemosphere* 316, 137814. <https://doi.org/10.1016/j.chemosphere.2023.137814>.
- Xue, W., Wang, L., Yang, Z., et al., 2023. Can clean heating effectively alleviate air pollution: An empirical study based on the plan for cleaner winter heating in northern China. *Appl. Energy* 351, 121923. <https://doi.org/10.1016/j.apenergy.2023.121923>.
- Yang, Y.T., 2022. Study on the impact of industrial agglomeration on environmental pollution. *Co-op. Econ. Sci.* (16), 4–6. <https://doi.org/10.13665/j.cnki.hzjjykj.2022.16.073> (in Chinese).
- Yang, X., Teng, F., 2018. The air quality co-benefit of coal control strategy in China. *Resour. Conserv. Recycl.* 129, 373–382. <https://doi.org/10.1016/j.resconrec.2016.08.011>.
- Zhang, C., Luo, L., Xu, W., et al., 2008. Use of local Moran's I and GIS to identify pollution hotspots of Pb in urban soils of Galway, Ireland. *Sci. Total Environ.* 398, 212–221. <https://doi.org/10.1016/j.scitotenv.2008.03.011>.
- Zhao, D., Lei, Y., Zhang, Y., et al., 2022. Analysis of vehicular CO₂ emission in the Central Plains of China and its driving forces. *Sci. Total Environ.* 814, 152758. <https://doi.org/10.1016/j.scitotenv.2021.152758>.
- Zhu, R., Zhang, C.J., Mei, M., 2018. The climate characteristics of atmospheric self-cleaning ability index and its application in China. *China Environ. Sci.* 38 (10), 3601–3610. <https://doi.org/10.19674/j.cnki.issn1000-6923.2018.0389> (in Chinese).
- Zhu, S., Gao, C., Song, K., et al., 2022. The changes in spatial layout of steel industry in China and associated pollutant emissions: a case of SO₂. *J. Environ. Manag.* 302, 114034 <https://doi.org/10.1016/j.jenvman.2021.114034>.